Published OnlineFirst October 12, 2017; DOI: 10.1158/1078-0432.CCR-17-2008

Clinical Cancer Research

CAR T Therapy Targeting ICAM-1 Eliminates Advanced Human Thyroid Tumors

Irene M. Min[1], Enda Shevlin[2], Yogindra Vedvyas[2,3], Marjan Zaman[2], Brian Wyrwas[1], Theresa Scognamiglio[4], Maureen D. Moore[1], Weibin Wang[1], Susan Park[2], Spencer Park[2,3], Suraj Panjwani[1], Katherine D. Gray[1], Andrew B. Tassler[5], Rasa Zarnegar[1], Thomas J. Fahey III[1], and Moonsoo M. Jin[1,2,3]

Abstract

Purpose: Poorly differentiated thyroid cancer and anaplastic thyroid cancer (ATC) are rare yet lethal malignancies with limited treatment options. Many malignant tumors, including papillary thyroid cancer (PTC) and ATC, are associated with increased expression of ICAM-1, providing a rationale for utilizing ICAM-1–targeting agents for the treatment of aggressive cancer. We developed a third-generation chimeric antigen receptor (CAR) targeting ICAM-1 to leverage adoptive T-cell therapy as a new treatment modality.

Experimental Design: ICAM-1 CAR T cells were applied to multiple malignant and nonmalignant target cells to investigate specific target cell death and "off-tumor" toxicity *in vitro*. *In vivo* therapeutic efficacy of ICAM-1 CAR T cells was examined in ATC mouse models established from a cell line and patient-derived tumors that rapidly develop systemic metastases.

Results: ICAM-1 CAR T cells demonstrated robust and specific killing of PTC and ATC cell lines *in vitro*. Interestingly, although certain ATC cell lines showed heterogeneous levels of ICAM-1 expression, addition of cytotoxic CAR T cells induced increased ICAM-1 expression such that all cell lines became targetable. In mice with systemic ATC, a single administration of ICAM-1 CAR T cells mediated profound tumor killing that resulted in long-term remission and significantly improved survival. Patient-derived ATC cells overexpressed ICAM-1 and were largely eliminated by autologous ICAM-1 CAR T cells *in vitro* and in animal models.

Conclusions: Our findings are the first demonstration of CAR T therapy against both a metastatic, thyroid cancer cell line and advanced ATC patient-derived tumors that exhibit dramatic therapeutic efficacy and survival benefit in animal studies. *Clin Cancer Res; 23(24); 1–15. ©2017 AACR.*

Introduction

Thyroid cancer is the most common malignancy of the endocrine system with an estimated 64,300 new cases being diagnosed in the United States in 2016 (1). This rate of diagnosis is increasing more rapidly than any other endocrine cancer in the United States (2). Most thyroid cancers are indolent and curable with standard treatments such as surgery, radioactive iodide (RAI) therapy, and thyroid stimulating hormone (TSH) suppression therapy for localized or regional disease. However, thyroid cancer patients can have widely different clinical outcomes depending on the pathological subtype. The follicular-derived thyroid cancers are divided into well-differentiated papillary thyroid cancer (PTC), follicular thyroid cancer (FTC), poorly differentiated thyroid carcinoma, and anaplastic thyroid carcinomas (ATC). The mortality rates of well-differentiated PTC (WDPTC), poorly differentiated PTC (PDPTC), and ATC are reported to be 3%–10%, 38%–57%, and close to 100%, respectively (1). Moreover, distant metastases occur at higher frequencies in PDPTC and ATC patients (representing approximately 5% of all thyroid cancer patients), reducing their 5-year survival to 55.3% from 99.9% for localized, well-differentiated tumors (3). The occurrence of ATC is fortunately rare and estimated to account for 2%–5% of all thyroid cancers, but when it does occur it is rapidly lethal with a median survival of 5 months and 1-year survival rate estimated at 10%–20% (4).

Research on targeted therapeutic interventions has focused on inhibiting aberrant pathways implicated in well-differentiated thyroid cancer, including RET/PTC translocations and BRAF point mutations (V600E) in PTC, and RAS point mutations in follicular and poorly differentiated thyroid carcinoma (4). VEGF and its receptors have also been extensively studied and targeted with multikinase inhibitor drugs like sorafenib, sunitinib, and lenvatinib. While these strategies hold promise for extension of progression-free survival, there is little evidence for improved overall survival of thyroid cancer patients treated with these drugs (1). Moreover, there are no systemic therapies (cytotoxic and/or targeted) that aid survival or quality of life in patients with metastatic ATC. Multikinase inhibitor drugs have shown very limited response in ATC patients except for a few reported anecdotal cases (5, 6), highlighting an urgent need for new treatment modalities.

[1]Department of Surgery, Weill Cornell Medicine, New York, New York. [2]Department of Radiology, Weill Cornell Medicine, 1300 York Avenue, New York, New York. [3]Department of Biomedical Engineering, Cornell University, Ithaca, New York. [4]Department of Pathology, Weill Cornell Medicine, 1300 York Avenue, New York, New York. [5]Department of Head and Neck Surgery, Weill Cornell Medicine, 1300 York Avenue, New York, New York.

Note: Supplementary data for this article are available at Clinical Cancer Research Online (http://clincancerres.aacrjournals.org/).

Corresponding Authors: Irene M. Min, Weill Cornell Medicine, 1300 York Avenue, New York, NY 10065. Phone: 212-746-5187; Fax: 212-746-6899; E-mail: irm2226@med.cornell.edu; Thomas J. Fahey III, tjfahey@med.cornell.edu; and Moonsoo M. Jin, moj2005@med.cornell.edu

doi: 10.1158/1078-0432.CCR-17-2008

Published OnlineFirst October 12, 2017; DOI: 10.1158/1078-0432.CCR-17-2008

Translational Relevance

Most thyroid cancers are indolent and curable with standard treatments; however, 5% to 10% of patients develop progressive disease that are metastatic and refractory to current treatments. Advanced, metastatic thyroid cancers have increased expression of ICAM-1, and we therefore developed a CAR T therapy targeting ICAM-1 for the treatment of aggressive thyroid cancer. Our study demonstrates the significant and durable efficacy of ICAM-1 CAR T for targeting ATC, one of the most aggressive and lethal solid tumors in humans. Furthermore, we showed that autologous ICAM-1 CAR T cells have significant therapeutic efficacy in animal models bearing ATC patient–specific tumors. Our CAR T-cell–based immunologic approach has potentially wide-ranging applications for the treatment of other solid cancers where there is a strong association between ICAM-1 expression and adverse prognosis.

Recently, cancer immunotherapy and in particular, adoptive cell therapy (ACT) have made significant technologic advancements leading to improvements in both efficacy and potential availability for the treatment of hematologic and solid tumors (7). Successful application of ACT using unmodified cytotoxic T cells (CTCs) relies upon isolation and *ex vivo* expansion of patient T cells, typically tumor infiltrating T cells (TIL) that recognize mutated or overexpressed tumor-associated antigens in an MHC-dependent manner. While successful in certain malignancies, most notably in melanoma (7), reliable extraction of TILs from a wider range of tumors is hampered by their low availability. Furthermore, tumors can downregulate MHC-I expression to render these T-cell receptor (TCR)-based therapies less effective (8). To enable effector T cells to target tumor antigens in a non-MHC–dependent manner, a chimeric antigen receptor (CAR) molecule that integrates antibody-derived antigen recognition via a single-chain fragment variable (scFv) and the zeta chain signaling domain from the TCR complex was devised in the late 1980s (9). Evolution of this design led to integration of additional signaling domains derived from costimulatory receptors such as CD28 and 4-1BB (10, 11) and these second and third generation CAR designs have shown remarkable success in hematologic cancers, particularly in B-cell malignancies (12, 13). Recently, positive outcomes have also been observed in clinical trials treating solid tumors, including neuroblastoma, melanoma, and synovial cell carcinoma (7).

With the intention of developing a CAR T therapy applicable to recurrent, advanced thyroid cancer patients with no alternative treatment options, we first validated ICAM-1 as a suitable antigen for CAR targeting by examining the correlation between ICAM-1 expression and malignant features in PTC and ATC. ICAM-1 is a member of the immunoglobulin superfamily, and is known to play a role in mediating cell–cell interactions such as leukocyte endothelial transmigration during inflammation (14). Under noninflammatory conditions, ICAM-1 expression is constitutively low and faintly detectable on endothelial cells. Increased ICAM-1 expression levels have been observed in multiple myeloma (15) and across many disparate carcinomas including breast (16), pancreas (17), and gastric (18) tumors, and are correlated with tumor progression and metastatic capability (19). Moreover, clinical trials support the safety and tolerability of targeting ICAM-1 using mAbs (20–24). Previous studies have shown that ICAM-1 expression is highly correlated with both the malignancy and metastatic status of thyroid tumors, as well as the V600E BRAF ($BRAF^{V600E}$) mutation (25, 26). The stark correlation between ICAM-1 expression and adverse prognostic outcomes in thyroid cancer patients suggests that ICAM-1 may serve as a therapeutic target for advanced, recurrent thyroid tumors.

Extending our prior study on ICAM-1–specific CAR T cells (27), here, we describe the development and preclinical application of ICAM-1 targeting third-generation CAR T cells that showed marked eradication of ATC cell lines and patient-derived primary ATC cells in an ICAM-1–specific manner. The surface expression levels of ICAM-1 on ATC cell lines and patient-derived primary ATC cells were sufficiently high to discriminate them from healthy primary tissue cells. Our CAR T-cell–based immunologic approach has potentially wide-ranging applications for the treatment of other solid cancers where there is a strong association between ICAM-1 expression and adverse prognosis.

Materials and Methods

Study approval

The studies were conducted in accordance with Declaration of Helsinki. Patient sample collection procedures were approved by the Weill Cornell Medicine Institutional Review Board, and patients' written consents were obtained prior to inclusion in the study.

Cell lines and primary cell culture

8505C and BCPAP cell lines were purchased from DSMZ. FRO and KHM-5M cell lines were kindly provided by Dr. James A. Fagin (Memorial Sloan-Kettering Cancer Institute, New York, NY). HEK 293T, HMEC-1, and HeLa cells were purchased from ATCC. Primary small airway epithelial cells (SAEC) from healthy donors and primary kidney glomerular microvascular endothelial cells (MVEC) were purchased from Lonza and Cell Systems, respectively. Cell culture growth media and culture conditions are described in detail in the Supplementary Methods section. Gene inactivation of ICAM-1 in 8505C was carried out using CRISPR plasmids available from Santa Cruz Biotechnology (sc-400098 and sc-400098-HDR). T-cell isolation from peripheral blood mononuclear cells and culture method has been described previously (27). Surgically resected fresh tumor tissues were cultured to establish patient-derived primary tumor cells with an endocrine pathologist (T. Scognamiglio) reviewing each case to ensure correct diagnosis.

CAR T vector construction, lentiviral production, and T-cell transduction

Engineering of the R6.5 scFv into a third-generation pLenti plasmid has been described previously (27). The sequence for rLuc was inserted into the vector using *Xba*I and *Sal*I restriction sites. Production of lentivirus particles and T-cell transduction was described previously (27).

Effector-to-target assay and cytokine analysis

For details, see Supplementary Methods.

Flow cytometry analysis for protein expression and cell cycle

For details, see Supplementary Methods.

Published OnlineFirst October 12, 2017; DOI: 10.1158/1078-0432.CCR-17-2008

Animals and tumor growth analysis

All animal studies were approved by Weill Cornell Medicine's Institutional Animal Care and Use Committee. Eight to 10-week-old female and male NOD-*scid*IL2Rg^{null} (NSG) mice (Jackson Laboratory) were used for xenograft experiments with ATC cells. GFP and fLuc-expressing 8505C (0.75×10^6 cells per mouse) and patient-derived ATC cells (0.36×10^6 cells per mouse) were intravenously injected to establish systemic metastasis establishment (28). Longitudinal measurements of 8505C tumor burdens were taken using a whole-body optical imager (In-Vivo Xtreme 4MP, Bruker) 15 minutes after intraperitoneal injection of 100 μL of 150 μg/mL D-luciferin (GoldBio). Total tumor burden was measured by generating full body region of interests (ROI) and integrating total flux of luminescence using Bruker Analysis software. GFP-expressing livers, spleen, heart, and lungs were extracted from mice and imaged with a whole-body optical imager (In-vivo F-Pro, Bruker). To track ICAM-1-CAR T cells expressing rLuc, mice were injected intravenously with 100 μL of RediJect Coelenterazine H (Perkin Elmer) and then immediately imaged using the In-Vivo Xtreme 4MP (Bruker).

IHC

For details, see Supplementary Methods.

Statistical analysis

Comparisons between categorical versus continuous variables were performed using the Mann–Whitney *U*/Kruskal–Wallis test as appropriate. The Spearman correlation test was used to compare continuous versus noncontinuous variables. To account for multiple-testing bias, the *P* value was adjusted using the Bonferroni correction. Statistical analysis was performed using Stata 14 or GraphPad Prism.

Results

Widespread overexpression of ICAM-1 in aggressive thyroid cancers

Previous reports have demonstrated a positive correlation between *ICAM-1* RNA and protein expression levels and the aggressive potential of PTC (25, 26), constituting ICAM-1 as a biomarker and a potential target for therapeutic interventions in thyroid cancer. PTCs are most commonly driven by two mutually exclusive somatic mutations, BRAF^{V600E} or mutated RAS (29). The BRAF^{V600E} mutation is an established marker associated with activation of MAPK and downstream ERK signaling, reduced iodine uptake (29), and advanced clinical staging in PTCs (30). Therefore, we investigated the characteristics of BRAF^{V600E} versus RAS-driven PTCs with coexistent *ICAM-1* overexpression (390 PTC patients in the Cancer Genome Atlas (TCGA) research database; ref. 29) to understand the underlying signaling and differentiation properties. Expression of *ICAM-1* mRNA in PTC positively correlated with an ERK activity metric (Spearman: 0.693, $P < 0.0001$; Fig. 1A). *ICAM-1* mRNA levels also associated better with tumors driven by BRAF^{V600E} compared with RAS mutations (BRAF^{V600E} and RAS-like tumors have negative and positive values in BRAF^{V600E}-RAS score (BRS), respectively; details in Supplementary Methods section; Fig. 1B). Moreover, *ICAM-1* mRNA expression in PTC patients was higher in those with the BRAF^{V600E} mutation compared with WT BRAF (Supplementary Fig. S1A). These data suggest that *ICAM-1* transcriptional control is linked to the activation of the BRAF–MAPK–ERK signaling pathway in PTC. Overexpression of *ICAM-1* in PTCs was associated with downregulation of thyroid-specific genes (Fig. 1C), increases in lymph node metastases (Fig. 1D), and extrathyroidal extension (Fig. 1E). PTC patients with high *ICAM-1* expression are more likely to suffer from recurrence (Fig. 1F) and to become refractory to treatments with conventional therapies such as RAI and TSH therapies (Fig. 1C).

Next, we obtained tissue sections from patients with ATC, the most lethal form of thyroid cancer, and examined ICAM-1 protein expression by histology. All ten ATC tumor specimens displayed high-grade (3^+) ICAM-1 staining with both cytoplasmic and membranous staining apparent in tumor cells [Fig. 1G; hematoxylin and eosin (H&E) images of corresponding tumor blocks are provided in Supplementary Fig. S2]. The fraction of tumor cells expressing ICAM-1 was also high, with seven of ten samples staining diffusely positive, thus defining them as category 3 (>60% of total tumor cells stain ICAM-1 positive). The remaining three samples were grouped in categories 1 and 2 (1 = 1%–29%; 2 = 30%–59% positive cells among entire tumor). The ICAM-1 intensity score (defined as multiplying the immunoreactivity score and staining score) for our ATC patient samples was 7.8 ± 2.1 SD), which is similar to that previously reported for RAI-refractory PTC and PDPTC (25). The prevalence of ICAM-1 staining in ATC bears striking contrast to neighboring tissues in the same tissue slice, which display structurally limited ICAM-1 immunoreactivity at the apical membrane of WDPTC and no ICAM-1 staining of normal thyroid follicles (Fig. 1G, right). The demonstration of increased ICAM-1 protein expression in ATC agrees with previously reported *ICAM-1* gene expression analyses that indicated significant differences in ICAM-1 expression between normal thyroid and PDPTCs (Supplementary Fig. S1B and S1C; refs. 31, 32). We further analyzed ICAM-1 IHC within eight distant metastases originating from thyroid cancers (Fig. 1H). Seven distant metastasis sites had category 3 ICAM-1 staining and four tissues displayed level 3^+, demonstrating an overall ICAM-1 intensity score of 6.9 ± 2.5 (SD). Interestingly, metastatic thyroid cancers across each pathologic subtype retained a similar ICAM-1 localization pattern. Distant metastases originating from WDPTC and follicular thyroid cancer displayed apical ICAM-1 staining, whereas poorly differentiated follicular carcinoma and ATC exhibited broad ICAM-1 distribution with circumferential membranous staining (Fig. 1H). Together, these findings demonstrate that ICAM-1 overexpression is a reliable molecular feature associated with PDPTC and ATC, and that circumferential membranous distribution of ICAM-1 is found in more advanced, metastatic thyroid cancers.

ICAM-1 overexpression is associated with highly aggressive ATC cells

We set out to investigate whether the level of ICAM-1 expression was linked to tumorigenic potency in established thyroid tumor cell lines. Several PTC and ATC cell lines were tested for their frequencies and levels of ICAM-1 expression by flow cytometry using the R6.5 mAb (33). The majority of thyroid cancer cell lines were ICAM-1 positive regardless of BRAF mutational status (Fig. 2A). Two ATC lines, 8505C and FRO, displayed heterogeneous expression of ICAM-1 with approximately 60% of both populations staining positive for ICAM-1 (Fig. 2A). Next, 8505C and FRO cells were stratified by sorting according to ICAM-1 expression to determine whether ICAM-1 levels were associated with tumorigenic potential. 8505C and FRO cells that were >85%

Published OnlineFirst October 12, 2017; DOI: 10.1158/1078-0432.CCR-17-2008

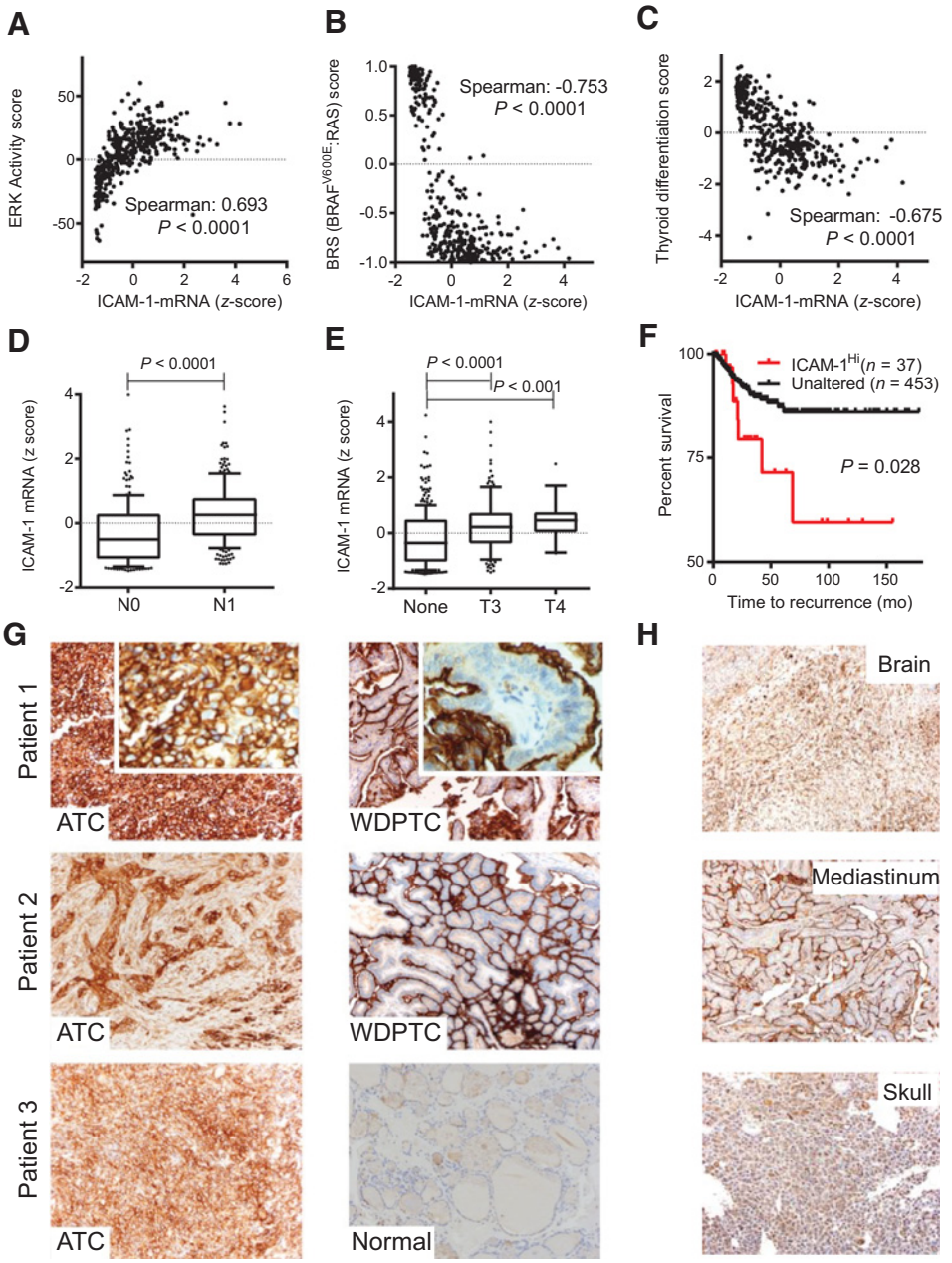

Figure 1.

ICAM-1 overexpression is associated with recurrent, advanced thyroid cancer cells. **A–C,** Spearman correlation analysis between *ICAM-1* mRNA expression and ERK activity (**A**), $BRAF^{V600E}$-RAS score (BRS; **B**), and thyroid differentiation score (**C**) were calculated using 390 PTC patient's genomics and clinical data available from TCGA analysis (29). Algorithms for these scores have been described previously in detail (29). **D** and **E,** Box plots compare tumor *ICAM-1* mRNA levels via the absence (N0) or presence (N1) of tumors metastases to nearby lymph nodes (**D**) and cancer associated with extrathyroidal extension (**E**, None, no extension; T3, minimal extension; T4, moderate/advanced/highly advanced extension; $n = 226$ and 232 for N0 and N1, respectively; $n = 338$, 133, and 18 for None, T3, and T4 groups, respectively). The solid, horizontal middle line in each Box plot indicates the median value; the upper and lower edges of each Box plot are the 75th and 25th percentiles, respectively, and the top and bottom short horizontal bars denote the 90th percentile and 10th percentiles respectively. Filled circles indicate outliers. Mann–Whitney (**D**) and Kruskal–Wallis (**E**) tests were used for determining statistical significance between groups. **F,** Kaplan–Meier plot indicating a significant difference between recurrence-free survival rate of 490 PTC patients with unaltered or overexpressed (z-score > 1.5) *ICAM-1* expression levels. **G,** Representative ICAM-1–specific IHC images of ATC patient-derived tissue. Well-differentiated PTC (WDPTC) or normal thyroid tissue images on the same slide are shown for comparison on the right. H&E images of the corresponding tissues are provided in Supplementary Fig. S2. Magnification, 20×. Inset images are 40× magnification. **H,** Representative ICAM-1 IHC results are shown for distant thyroid tumor metastases at 20× magnification.

ICAM-1–positive (designated as $ICAM\text{-}1^{Hi}$) maintained their pattern of ICAM-1 expression during extended culture to at least 10 passages (Fig. 2B). 8505C-$ICAM\text{-}1^{Hi}$ and FRO-$ICAM\text{-}1^{Hi}$ cells were found to be more refractory to treatment with the BRAF inhibitor vemurafenib, by 4.6- and 17.7-fold respectively, compared with their parental (par) counterparts (Fig. 2C). Elevated vemurafenib resistance was also observed in a colony formation assay, which demonstrated higher and larger colony-forming units in $ICAM\text{-}1^{Hi}$ populations compared with parental cells (Fig. 2D). Cell-cycle analysis showed that both 8505C-$ICAM\text{-}1^{Hi}$ and FRO-$ICAM\text{-}1^{Hi}$ cells had a higher percentage of cells at the proliferating stage (S–G_2/M and S) relative to parental cells (Fig. 2E; Supplementary Fig. S3). Taken together, ICAM-1–positive 8505C and FRO cells are distinguished by an increased resistance to vemurafenib and an elevated rate of proliferation, suggesting that ICAM-1 can serve as a biomarker for the aggressive nature of ATC cells.

ICAM-1–targeting CAR T shows specific killing of malignant thyroid cells

As the aggressive and vemurafenib-resistant features of ATC correlate with ICAM-1 overexpression, we developed an immunotherapeutic strategy specifically targeting ICAM-1 as a novel treatment for refractory ATC. To molecularly target ICAM-1, we

Published OnlineFirst October 12, 2017; DOI: 10.1158/1078-0432.CCR-17-2008

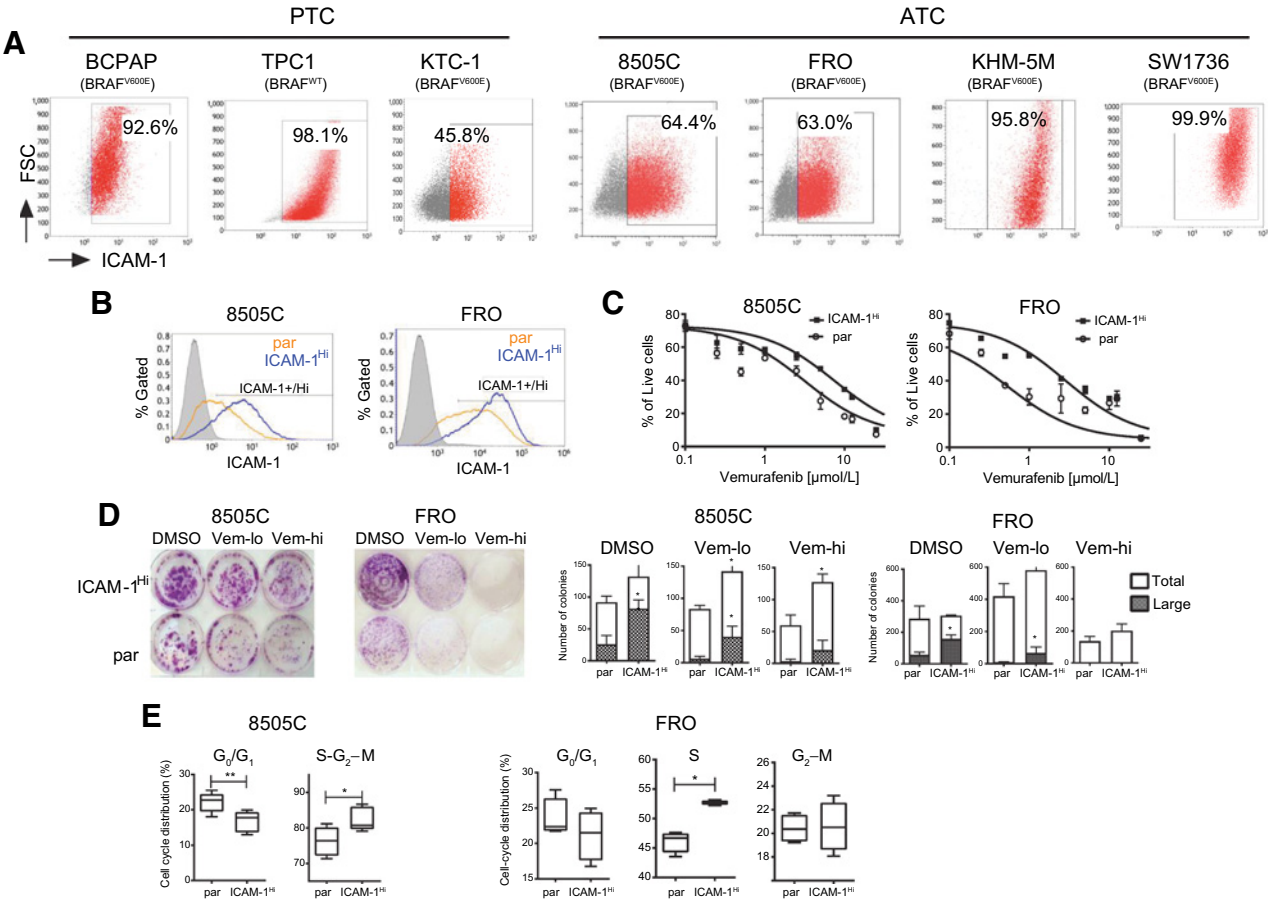

Figure 2.

ICAM-1$^+$ is a biomarker for ATC. **A,** Representative flow cytometry plots showing ICAM-1 expression in PTC (BCPAP, TPC-1, KTC-1) and ATC (8505C, FRO, KHM-5M, SW1736) cell lines. All cell lines except TPC-1 harbor the BRAF^{V600E} mutation. Boxes indicate cells that were determined to be ICAM-1 positive (shown as red dots) based on isotype controls. **B,** ICAM-1 histogram plots of parental (par; orange lines) and FACS sorted (ICAM-1^{Hi}; blue lines) 8505C (left) and FRO cells (right). Gray histograms indicate isotype control stained par cells. **C,** MTT analysis showing the percentage of live cells remaining after 72 hours of vemurafenib treatment in par and ICAM-1^{Hi} cells isolated from 8505C (left) and FRO (right). IC_{50} values for ICAM-1^{Hi} cells relative to par were increased 4.6-fold and 17.7-fold in 8505C and FRO cells, respectively ($n = 3, 6$). **D,** Representative images of cell colonies formed after treatment with vehicle DMSO, low (1.5 and 2.5 μmol/L for 8505C and FRO, respectively) and high (2.5 and 10 μmol/L for 8505C and FRO, respectively) doses of vemurafenib (left). Quantification of the total number of colonies and colonies of large size (>2 mm diameter) is shown on the right (*, $P < 0.05$ by Mann–Whitney test, $n = 4$). **E,** Summary of cell-cycle distribution between G_0–G_1 and proliferative phases of par and ICAM-1^{Hi}-enriched 8505C (left) and FRO (right) cells (*, $P < 0.05$; **, $P < 0.01$ by Mann–Whitney test; $n = 6, 8$ for 8505C and $n = 4$ for FRO).

inserted an scFv derived from the ICAM-1–specific R6.5 mAb into a third-generation CAR construct comprised of intracellular CD3ζ, CD28, and 4-1BB (CD137) signal transduction domains (Fig. 3A; refs. 11, 27). An additional *Renilla* luciferase (rLuc) reporter gene was also inserted downstream of the CAR via a P2A ribosomal skipping sequence for CAR T-cell tracking *in vivo*. Lentiviral transduction of this ICAM-1–targeting CAR construct (hereafter referred to as ICAM-1 CAR) into CD3$^+$ T cells yielded between 20% and 60% CAR expression, which could be increased to approximately 100% after CAR-based sorting using an anti-mouse F(ab′)2 antibody (Fig. 3B). ICAM-1 CAR expression on primary T cells did not alter the CD4:CD8 ratio or T-cell proliferation (Supplementary Fig. S4), suggesting a lack of self-directed cytotoxicity despite endogenous ICAM-1 expression on primary T cells.

We tested the ability of ICAM-1 CAR T cells to eliminate PTC, ATC, and control cells with and without ICAM-1 expression using varying ratios of T cells (effector) to target cells (Fig. 3C). For this assay, we first established target cell lines with stable expression of GFP and firefly luciferase (fLuc) via transduction with a fLuc-F2A-GFP lentivirus and flow cytometry–based sorting for GFP$^+$ cells. PTC BCPAP cells, which are mostly ICAM-1$^+$, were eliminated fastest by ICAM-1 CAR T cells relative to 8505C and FRO cells which have lower ICAM-1 expression (Fig. 3C). HEK 293T cells, with diminutive ICAM-1 expression, were largely protected from ICAM-1 CAR T cells, displaying slow, gradual cell death from nonspecific T-cell activity. Compiled data from E:T assays at the 2.5:1 E:T ratio demonstrated that ICAM-1 CAR T lysed BCPAP, HeLa, and FRO cells with similar kinetics followed by 8505C cells at a reduced rate (Fig. 3D). Mock-transduced T cells exhibited minimal effects on all tested cells except for BCPAP (Fig. 3D). At the 20-hour time point, approximately 40% of 8505C cells remained viable after exposure to ICAM-1 CAR T cells, a percentage that equates with the level of ICAM-1 expression on 8505C

Published OnlineFirst October 12, 2017; DOI: 10.1158/1078-0432.CCR-17-2008

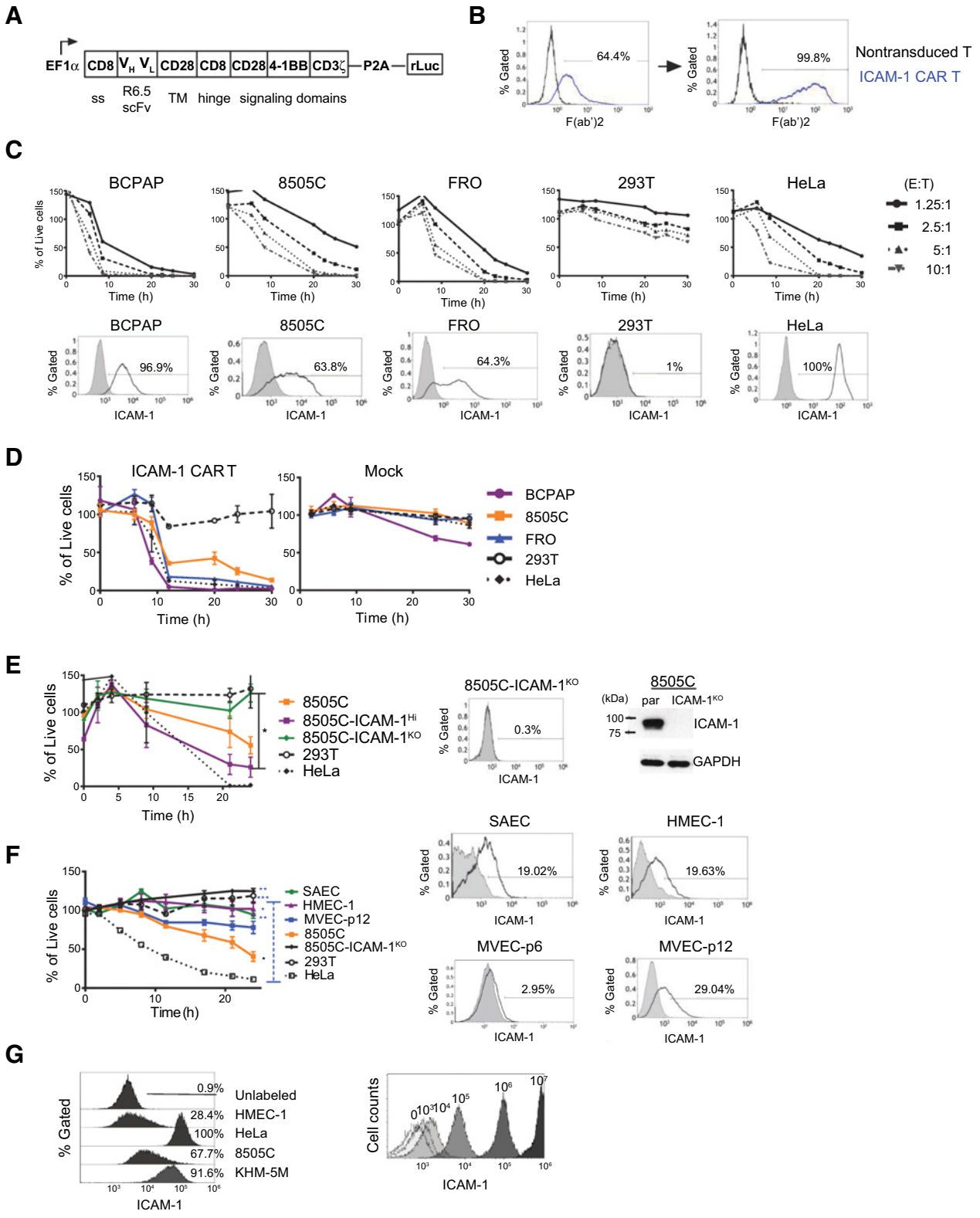

Figure 3.

ICAM-1–targeting CAR T activity is specific to the ICAM-1–expressing target cells. **A,** Schematic demonstrating the ICAM-1 CAR T construct. **B,** Histogram plots demonstrating CAR expression in ICAM-1 CAR T cells was detected using a F(ab′)2 antibody before (left) and after (right) sorting via F(ab′)2. **C,** The percentages of live target cells remaining after exposure to ICAM-1 CAR T plotted over time (top). (*Continued on the following page.*)

Published OnlineFirst October 12, 2017; DOI: 10.1158/1078-0432.CCR-17-2008

cells (Figs. 2A and 3C). The extent of ICAM-1 CAR T targeting of 8505C cells was dependent upon the level of ICAM-1 expression, as evidenced by the faster killing of 8505C-ICAM-1^{Hi} cells compared with their lower ICAM-1–expressing parental counterparts (Fig. 3E). Genetic disruption of ICAM-1 via CRISPR/Cas9 in 8505C cells (referred to as 8505C-ICAM-1^{KO}) abolished ICAM-1 CAR T–mediated killing of 8505C cells, thus demonstrating the targeting specificity of this treatment strategy *in vitro* (Fig. 3E). Abolished ICAM-1 expression in 8505C-ICAM-1^{KO} cells was confirmed by flow cytometry and Western blot analysis (Fig. 3E, right).

To address the potential for "on-target, off-tumor" killing by ICAM-1 CAR T cells, we investigated whether ICAM-1 CAR T could target healthy human cells with normal ICAM-1 expression (34). We chose MVECs and SAECs that have the highest ICAM-1 expression among normal tissues according to the Human Protein Atlas database (34). In contrast, these tissues have also been reported to stain poorly for ICAM-1 by IHC (16, 35). By immunostaining with mAb R6.5, we found that SAECs, early passage (passage 6) MVECs, and late passage (passage 12) MVECs, were approximately 19%, 3%, and 29% ICAM-1 positive, respectively (Fig. 3F, right). As an additional comparison, we also used immortalized dermal microvascular endothelial cells (HMEC-1), which were 20% ICAM-1 positive. The levels of ICAM-1 expression in primary healthy cells were 2- to 10-fold lower than the 8505C and FRO ATC lines (Fig. 3C and F). In turn, the level of ICAM-1 CAR T cell–mediated killing of the healthy lung, kidney tissue cells, and HMEC-1 cells was significantly lower than that observed for 8505C and HeLa cells. Indeed, the cytotoxicity directed against healthy tissue was not significantly different from that of the ICAM-1–negative cells, HEK 293T and 8505C-ICAM-1^{KO} (Fig. 3F, left). Therefore, the magnitude of ICAM-1 CAR T cytotoxicity was reflective of the frequency and the extent of ICAM-1 expression in target cells with nonmalignant, ICAM-1–low cells, exhibiting limited susceptibility.

To define the threshold level of ICAM-1 expression that is required for effectual cytotoxicity of ICAM-1 CAR T cells, we estimated the number of ICAM-1 molecules expressed on target cell surfaces by comparing R6.5 antibody binding to cells with the signal obtained from 8-μm latex beads coated with known amounts of R6.5 antibodies (Fig. 3G). From this comparison, we estimated that the primary healthy tissue cells and ATC lines display approximately 10^4 and 10^5 ICAM-1 molecules on their cell surfaces, respectively, suggesting a requirement for expression of 10^5 ICAM-1 surface molecules per cell to enable efficient engagement and killing by ICAM-1 CAR T cells. Therefore, due to ICAM-1 CAR T's ability to discriminate between target thyroid cancer cells and healthy primary tissue cells, ICAM-1 CAR T should exhibit a sufficiently high therapeutic index for clinical use.

Surface ICAM-1 expression in thyroid cancer cells is modulated by IFNγ, which affects the efficiency of ICAM-1 CAR T cytotoxicity

8505C cells exhibited slower ICAM-1 CAR T–induced death compared with BCPAP and HeLa cells with approximately 40% of targets remaining alive at the 20- to 24-hour time points when cocultured at a 2.5:1 E:T ratio (Figs. 3D and 4A). Interestingly, the viable 8505C cells that remained after incubation with ICAM-1 CAR T cells at 18 hours displayed an elevated level of ICAM-1 expression (7.5-fold increase in MFI) relative to nonexposed cells (Fig. 4B). A similar elevation of ICAM-1 expression was measured in 8505C, BCPAP, and FRO cells after incubation in preconditioned media collected from 18-hour cocultures of 8505C cells with ICAM-1 CAR T cells suggesting that soluble factors released into the media by cytotoxic CAR T cells are responsible for ICAM-1 induction (Fig. 4C). A hallmark of CTC activity is secretion of the Th1 cytokine IFNγ (11). We therefore measured the concentration of secreted IFNγ during ICAM-1 CAR T coculture with target cells during the E:T assays. Release of IFNγ by CAR T cells was highest when cocultured with 8505C-ICAM-1^{Hi} and HeLa cells, and remained at background levels with 8505C-ICAM-1^{KO} and HEK 293T cells (Fig. 4D). Furthermore, addition of exogenous IFNγ into thyroid cancer cell monocultures induced ICAM-1 expression in a dose-dependent fashion, thus identifying IFNγ as a critical soluble factor responsible for ICAM-1 induction in target cells (Fig. 4E).

Addition of IFNγ at a concentration of 1×10^4 pg/mL was sufficient to induce an approximate 10-fold increase in ICAM-1 expression ($\sim 10^6$ molecules per cell) in all tested thyroid cancer cells (Figs. 3G and 4E). The levels of IFNγ secreted by ICAM-1 CAR T cells upon exposure to target antigen were also within a range capable of elevating ICAM-1 to levels observed by exogenous IFNγ addition. In contrast, ICAM-1 expression in HEK 293T cells was absent upon addition of supernatant from HeLa cells targeted by ICAM-1 CAR T (Fig. 4C) or by administration of exogenous IFNγ (Fig. 4E). Addition of a supraphysiologic concentration of IFNγ to early passage MVEC cells induced an approximately 2- to 3-fold increase in MFI (Fig. 4E). These data suggest that thyroid cancer cells are hyper-responsive to IFNγ-induced ICAM-1 elevation compared with nonmalignant, healthy cells. In addition, E:T assays with IFNγ-stimulated target cells verified that ICAM-1 CAR T cells demonstrated increased cytotoxicity against 8505C cells (Fig. 4F). In contrast, MVECs displayed no difference in cytolysis by nontransduced T or ICAM-1 CAR T cells after administration of IFNγ except for the increased death of cells treated with IFNγ

(*Continued.*) Values were normalized to target cells with no T-cell addition. The E:T ratio was incremented by a factor of 2 from 1.25:1 to 10:1. (bottom) Flow cytometry plots indicating the level of ICAM-1 expression in target and control cells after staining with the R6.5 anti-ICAM-1 antibody. Gates for ICAM-1^+cells were determined on the basis of staining with isotype control (gray-filled histogram). **D,** Compilation of the percentages of live target cells remaining after exposure to ICAM-1 CAR T and mock transduced T cells plotted over time (normalized against no T-cell addition group, $n = 4$–7 per target cell line). **E,** ICAM-1 CAR T cytotoxicity against parental 8505C cells and 8505C cells with high (ICAM-1^{Hi}) or minimal (ICAM-1^{KO}) ICAM-1 expression. The plotted percentages of live cells were normalized against corresponding target cells incubated with nontransduced T cells to minimize the T-cell alloreactivity. A statistical difference was observed between the number of live 8505C-ICAM-1^{KO} and 8505C-ICAM-1^{Hi} cells remaining at the 24- and 30-hour timepoint (*, $P < 0.05$ by Dunn multiple comparison test). 8505C-ICAM-1^{KO} cells were generated using CRISPR/Cas9, and ICAM-1 expression levels were analyzed by flow cytometry and Western blot analysis (right). **F,** ICAM-1 CAR T cytotoxicity against normal primary cells along with control target cells. Membrane-bound ICAM-1 expression on normal primary cells was characterized by flow cytometry (right). Statistical differences were analyzed between the SAEC, HMEC-1, and 293T cells relative to HeLa cells. 8505C cells were compared to 293T cells (*, $P < 0.05$; **, $P < 0.01$; ***, $P < 0.001$ by Dunn's multiple comparison tests at 24 hr) ($n = 3$–6 per target cells). **G,** Histograms of latex beads coated with a fixed number of R6.5 anti-ICAM-1 antibodies were analyzed by flow cytometry on the right. Histograms plots for various target cells with R6.5 antibody on the left were used to estimate the number of ICAM-1 molecules.

Published OnlineFirst October 12, 2017; DOI: 10.1158/1078-0432.CCR-17-2008

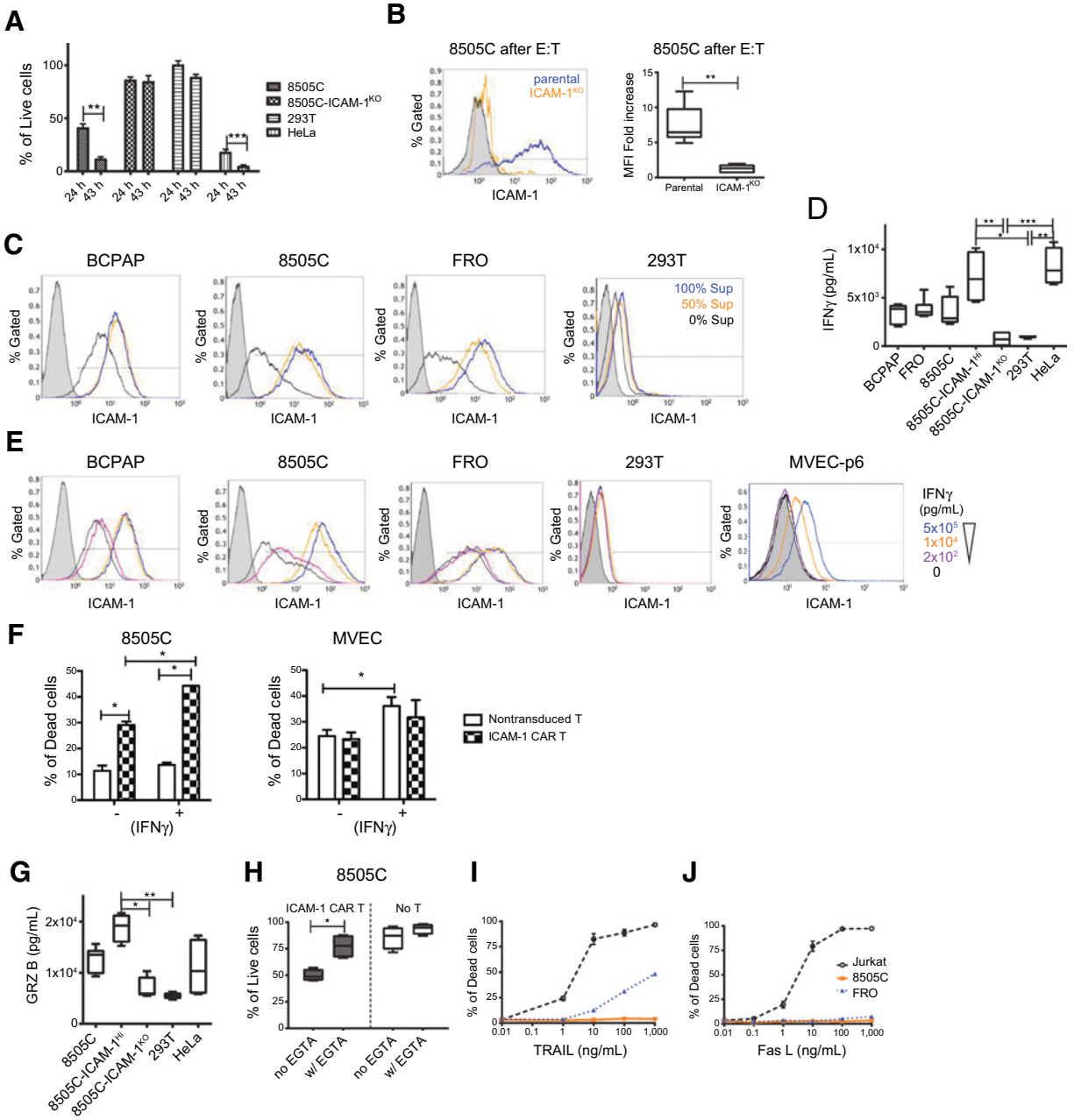

Figure 4.

ICAM-1 expression on thyroid cancer cells is IFN-γ–inducible by enhancing target susceptibility to ICAM-1 CAR T. **A,** The percentages of viable target cells remaining after coculturing with ICAM-1 CAR T cells were compared between 24-hour and 43-hour timepoints ($n = 6$–9 per target cells). **B,** After an 18-hour coincubation with ICAM-1 CAR T cells, 8505C (blue line) and 8505C-ICAM-1^{KO} (orange line) cells were collected and stained for ICAM-1 expression in live cells by flow cytometry (left). 8505C cells stained with isotype control are shown by gray filled histogram. Quantitation of the fold increase of ICAM-1 mean fluorescence intensity (MFI) is shown on the right relative to nonexposed cells ($n = 6$ per target cells). **C,** Representative flow cytometry plots show thyroid cancer cell ICAM-1 expression after 18-hour culture in media spiked with supernatant derived from E:T experiments using ICAM-1 CAR T. Supernatants from the ICAM-1 CAR T: target cell assay were collected and added to the indicated target cells with no dilution (blue line), 50% dilution (orange line), or no addition (black line) to the culture media. **D,** The IFNγ levels in supernatants collected from E:T assays involving ICAM-1 CAR T against indicated target cells were measured using ELISA ($n = 4$–8). Nontransduced T cells cultured with the same target cells produced levels of IFNγ that were below the limit of detection. **E,** Flow cytometry analysis demonstrating ICAM-1 expression changes in thyroid cancer and control cells upon direct administration of exogenous, serially diluted IFNγ (pg/mL). **F,** The percentages of cell death observed in untreated and IFNγ (1×10^4 pg/mL) added target cells were compared after addition of nontransduced T and ICAM-1 CAR T cells using flow cytometry analysis ($n = 3$). **G,** The concentration of secreted granzyme B from an ICAM-1 CAR T: target cell assay ($n = 4$–6) per condition. **H,** 4 mmol/L EGTA was added to E:T assay media to inhibit the perforin/granzyme cytotoxic pathway ($n = 4$ per group). **I,** Anaplastic thyroid cancer resistance to TRAIL-induced death. **J,** Anaplastic thyroid cancer resistance to FasL-induced death. The Jurkat T cell line served as a positive control for both treatments ($n = 3$–4 per condition).

Published OnlineFirst October 12, 2017; DOI: 10.1158/1078-0432.CCR-17-2008

relative to untreated cells. IFNγ-mediated induction of ICAM-1 expression may therefore increase the therapeutic potency of ICAM-1 CAR T cells against thyroid cancer cells while preserving tolerance of nonmalignant, normal tissues.

The direct cytotoxic effects mediated by CAR T cells derive from their release of soluble factors such as perforin and granzymes, in addition to TNF death receptor signaling triggered by direct cell-to-cell contacts. The level of granzyme B secretion was found to mirror the rate of ICAM-1–dependent target cell killing, which was highest in 8505C-ICAM-1^{Hi}, followed by parental 8505C, and negligible in the 8505C-ICAM-1^{KO} cells (Fig. 4G). The dependence upon perforin/granzyme B–mediated target killing was also validated by the substantial inhibition of CAR-mediated cytotoxicity by addition of EGTA to E:T cocultures (Fig. 4H). In contrast, activation of the TNF death receptor pathway by exogenous addition of its ligand, TRAIL, had little effect on 8505C cell death, while gradual killing of FRO cells was observed with increasing concentrations of TRAIL (Fig. 4I and J). We therefore confirmed that the degree of ICAM-1 CAR T cytotoxicity is commensurate with the levels of surface ICAM-1 expression in target cells. Furthermore, we identified IFNγ as a crucial cytokine that can augment CAR T cytotoxicity by preferentially acting upon thyroid cancer cells.

CAR T cells targeting ICAM-1 achieve rapid and enduring tumor eradication *in vivo*

To evaluate the antitumor efficacy of ICAM-1 CAR T *in vivo*, we utilized systemic xenografts of human ATC 8505C cells in immunodeficient NOD-*scid*IL2Rg^{null} (NSG) mice (28). To track and quantitate the growth of ATC in mice, we used parental 8505C cells transduced and FACS sorted to express GFP and fLuc with approximately 100% purity. A total of 0.75×10^6 8505C cells were injected intravenously into each NSG mouse, with primary tumors localizing prominently in the lungs (Fig. 5A). With unimpeded growth, tumors gradually metastasize to other organs including the bones and liver, resulting in death within one month (median survival is 28 days). Treatment occurred on day 14 postxenograft with mice receiving an intravenous infusion of either 3×10^6 T cells transduced with an ICAM-1 CAR lentivirus (unsorted with 30%–40% transduction levels) or an equal infusion of 3×10^6 nontransduced T cells. A third group received no treatment. The specific cytotoxicity of administered ICAM-1 CAR T cells were validated *in vitro* and their CD4:CD8 ratios were additionally confirmed to be comparable with nontransduced T cells (Supplementary Fig. S5). At day 5 posttreatment with ICAM-1 CAR T, mice showed signs of tumor signal decrease and recovery of body weight, culminating in complete tumor eradication and weight rebound within 12 days of treatment (Fig. 5A–C). The observed remission was durable such that ICAM-1 CAR treated mice exhibited a significant and substantial increase in survival (Fig. 5D). Nontransduced T cells demonstrated minimal tumor killing in mice, except for the occasional instances of donor T-cell alloreactivity. *Ex vivo* fluorescence images of harvested organs taken 1 month after ICAM-1 CAR T treatment demonstrated that tumor lesions were strikingly diminished in the lungs and livers in contrast to the untreated group (Fig. 5E). The reduction of tumor burden mediated by ICAM-1 CAR T cells in the lungs was also evidenced by their lower (normal) weight compared with the 2.2-fold higher weight of the same organs from the untreated group (Supplementary Fig. S6).

The macroscopic descriptions of tumor eradication by ICAM-1 CAR T cells were validated at the cellular level by flow cytometry and IHC analyses. Examination of whole lung and liver tissue from ATC xenografted mice treated with ICAM-1 CAR T showed negligible levels of GFP$^+$ tumor cells, in striking contrast to untreated groups in which approximately 18% and 4% of live cells were identified as GFP$^+$ in the lungs and liver, respectively (Fig. 5F). IHC analysis revealed that $\leq$1% of the lung and liver tissues retained GFP$^+$ tumor cells at 70–80 days after a single administration of ICAM-1 CAR T cells (Fig. 5G). Meanwhile, human CD3$^+$ T cells were still detectable in various organs at day 72 (Fig. 5F; Supplementary Fig. S7A), which agreed with the assessment of CAR T cell persistence evidenced by whole body imaging of rLuc–expressing CAR T cells (Supplementary Fig. S7B). These findings demonstrate the ability of ICAM-1 CAR T cells to mediate potent and enduring antitumor activities, leading to tumor eradication and significant improvements in long-term survival in ATC xenograft mouse models.

Autologous ICAM-1 CAR T eliminates thyroid cancer patients' tumor cells *in vitro* and *in vivo*

Acknowledging the modeling deficiencies of using healthy donor-derived T cells to treat allogeneic, cell line–derived tumor cells, we wanted to test the therapeutic efficacy of ICAM-1 CAR T cells in a more realistic setting using patient-derived tumors and autologous T cells. We therefore initiated primary cultures of fresh tumor specimens derived from PDPTC and ATC thyroid cancer patients. Aggressive tumors with known recurrences were chosen. Specifically, PDPTC cells were extracted from the metastatic lymph node of a patient who developed local recurrence after suppressive hormonal therapy and RAI treatment; this same patient also went on to develop enlarging pulmonary metastases and became debilitated from treatment and disease burden. ATC cells were harvested from the primary tumor of a patient who developed pulmonary metastases within three months of treatment with chemotherapy and external beam radiation. Surgically removed tumor blocks were IHC stained for ICAM-1, which exhibited high-grade ICAM-1 expression (3$^+$) in agreement with our previous results (Figs. 1G and 6A and B and Fig.). After 2–5 days of primary culture, the majority of PDPTC and ATC cells were dual positive by flow cytometry for surface expression of ICAM-1 and epithelial cell adhesion molecule (EPCAM), a marker for follicular epithelial cells (Fig. 6A and B). While PDPTC tissues indicated sparse (~10%) ICAM-1 expression by IHC, expression after subculturing was over 90%. Several factors may account for such a discrepancy in ICAM-1 expression including unintended induction of ICAM-1 due to culturing conditions and selective growth of ICAM-1$^+$ cells in culture.

Next, we tested the cytotoxic activity of autologous ICAM-1 CAR T cells against patient-derived tumor cells. ICAM-1 CAR T cells obtained from a PDPTC patient eliminated autologous thyroid tumor cells with similar kinetics to HeLa cells with no reactivity toward HEK 293T cells (Fig. 6A). Similarly, ICAM-1 CAR T cells derived from an ATC patient lysed autologous primary tumor cells, HeLa, and 8505C cells at comparable rates, achieving near 100% killing by 48 hours. The rate of killing was somewhat slower in the autologous setting compared to the previously observed response from healthy donor–derived ICAM-1 CAR cells, which showed faster killing of target cells with high ICAM-1 expression (Fig. 3E and F).

Published OnlineFirst October 12, 2017; DOI: 10.1158/1078-0432.CCR-17-2008

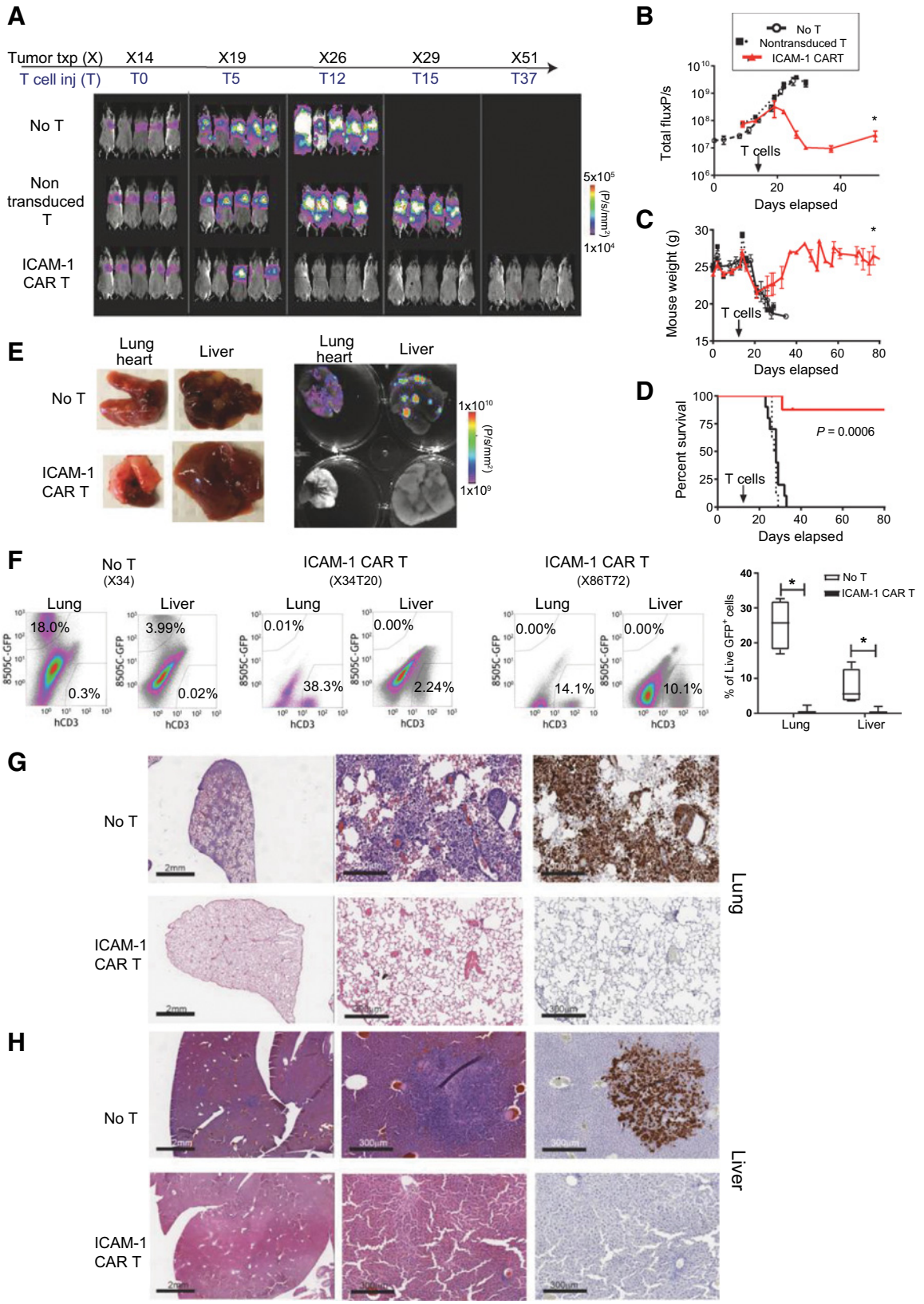

Published OnlineFirst October 12, 2017; DOI: 10.1158/1078-0432.CCR-17-2008

To more closely examine and predict patient-specific efficacy of ICAM-1 CAR T therapy, we further established ATC patient–derived xenograft models in NSG mice. The patient-derived ATC tumors carried a mutational profile (mutations in NRAS, p53, and PTEN) that differed from that of 8505C, which carries known mutations in $BRAF^{V600E}$ and TP53 (36). ATC patient–derived tumor cells were transduced with the fLuc-F2A-GFP lentivirus obtaining GFP expression of 15%. ATC cells were first injected subcutaneously into bilateral flanks, which, over a period of one month, grew to form uneven tumor masses (Supplementary Fig. S8A). Tumors harvested from xenografted mice displayed distinct pleiomorphism, hyperchromatism, increased nuclear to cytoplasmic ratio, and multiple mitoses, which are known features of undifferentiated thyroid cancer cells (Supplementary Fig. S8B). At this stage, the percentages of GFP^+ cells in the bulk tumor were reduced to approximately 5%, yet GFP^+ tumor cells were found to retain the same EPCAM/ICAM-1 profile as the original primary patient cell cultures (Supplementary Fig. S8C).

Patient cells derived from subcutaneous tumors (as in Supplementary Fig. S8) were expanded in culture for additional 2 passages, and intravenously injected to produce metastatic tumor xenografts in NSG mice. Similar to the 8505C cell line xenografts, patient-derived ATC cells grew predominantly in the lungs (Fig. 6C and D). Because of the difficulty in obtaining primary tumor cells with sufficiently high GFP and fLuc expression for tracking tumor growth by luminescence imaging, we used MRI to detect the tumors in lungs, and quantified the volume fractions of tumor to the pulmonary cavity in untreated and ICAM-1 CAR T–treated mice (Fig. 6C). Lung tumor burden at 67–72 days after xenografts was significantly reduced in mice treated with a single infusion of autologous ICAM-1 CAR T (>1.5 million cells per mouse) compared with untreated (No T) controls. Lung tissues obtained from untreated mice showed tumor growth characteristics that were either diffuse, nodular, or both in the lung parenchyma and pleura (Fig. 6D). In comparison, the alveolar space was almost tumor free in CAR T–treated lung tissues with small remnant tumors found in pleural and perivascular regions. The number of visible metastatic tumor nodules within the lung lobes of ICAM-1 CAR T–treated mice was significantly reduced compared with non-CAR controls as measured by IHC (Fig. 6D). Finally, ICAM-1 CAR T treatment led to a significant improvement in the overall survival of ATC xenografted mice compared with nontreated controls that lasted approximately 70–80 days posttreatment (Fig. 6E). During this period, whole body luminescence imaging confirmed persistence of rLuc-positive CAR T cells prominently in the head and the spleen, and weakly in lungs and other organs (Supplementary Fig. S9).

Discussion

Encouraged by impressive clinical developments of CAR T therapy for treatments of hematologic malignancies, we sought to develop a CAR T therapeutic strategy for advanced thyroid cancers. Here, we demonstrated the therapeutic potential of CAR T cells recognizing ICAM-1 for the treatment of a metastatic, aggressive thyroid cancer such as ATC, which is known to have one of the shortest median survival times among all solid tumors. Remarkably, we also showed that ICAM-1 CAR T cells manufactured from the peripheral blood of a patient already compromised by ATC led to a significant reduction of tumor burden and led to prolonged overall survival of animals xenografted with autologous ATC tumors. To our knowledge, our approach is the first report utilizing patient-derived CAR T cells for the treatment of patient-derived, autologous solid tumor xenografts. This novel modeling approach can be used to aid the optimization of clinical protocols regarding treatment doses, timing, and administration of additional adjuvants to maximize therapy efficacy and safety.

Our rationale for developing therapeutics targeting ICAM-1 for treatment-refractory thyroid cancer is based upon several observations. ICAM-1 is significantly elevated in ATC and other thyroid cancer subtypes that metastasize to distant organs, thus presenting ICAM-1 as a useful prognostic marker for metastatic, aggressive thyroid cancer subtypes. From the analyses of TCGA PTC genomics in combination with clinical data, the level of *ICAM-1* expression was found to correlate with aggressive tumorigenic features. This correlation was also experimentally validated in our study across multiple thyroid cancer cell lines. Moreover, ICAM-1–targeting therapy has potential applications for the treatment of other malignancies, including pancreatic ductal adenocarcinoma (17), breast cancer (16), multiple myeloma (37), and gastric tumors (18), where ICAM-1 surface expression is also significantly elevated compared to normal tissues. Along with thyroid carcinoma, TCGA studies indicated that overall patient survival was shorter when levels of *ICAM-1* mRNA were upregulated in glioblastoma multiforme, renal clear cell carcinoma, renal papillary cell carcinoma, and hepatocellular carcinoma (Supplementary Fig. S10; refs. 35, 38).

To target tumor cells with high surface ICAM-1 expression, we adopted an scFv from R6.5 (33), a murine mAb against ICAM-1, and fused it with the transmembrane and intracellular signaling

Figure 5.

ICAM-1 CAR T cells show robust and enduring tumor eradication in ATC xenograft models. **A,** Representative total body bioluminescence images of $fLuc^+$ 8505C xenografted NSG mice following ICAM-1 CAR T cell administration. Control groups include untreated and nontransduced T cell–administered mice. **B,** Quantitation of total body bioluminescence units in individual mice from (**A**) (no T cell group = open circle, non-transduced T cells = solid square, ICAM-1 CAR T = red triangle; * marks $P < 0.05$, $n = 8$–10 per group). **C,** Summary of body weight changes in mice left untreated or after treatment with nontransduced T cells or ICAM-1 CAR T cells (* marks $P < 0.05$). **D,** Survival curves of 8505C xenografted mice comparing no treatment, treatment with nontransduced T cells, and treatment with ICAM-1 CAR T cells until 80 days postxenograft. Statistical differences between different treatments were analyzed by Kaplan–Meier ($n = 8$–10 per group). **E,** (left) Gross inspection of 8505C xenograft metastatic organs (lung, liver) taken 20 days after ICAM-1 CAR T treatment compared with untreated mouse organs. (right) *Ex vivo* GFP fluorescence images of the organs merged with bright field images. Scale bar is shown on the right. **F,** (left) Flow cytometry plots showing analysis of percentages of GFP^+ 8505C (*y*-axis) and human $CD3^+$ T cells in indicated organs extracted from untreated and ICAM-1 CAR T treated 8505C xenografted mice (20 and 72 days after T cell administration). Bottom, compilation of the frequency of live, GFP^+ 8505C cells observed in the lung and liver with and without ICAM-1 CAR T treatment. **G** and **H,** Representative IHC images showing H & E staining of low (left) and high (middle) magnifications of lung (**G**) and liver (**H**) tissues isolated from xenografted mice receiving no T-cell (top) or ICAM-1 CAR T (bottom) treatment. The adjacent sections were stained for GFP to identify tumor cells (right). Scale bar = 2 mm (left), 300 μm (middle, right).

Published OnlineFirst October 12, 2017; DOI: 10.1158/1078-0432.CCR-17-2008

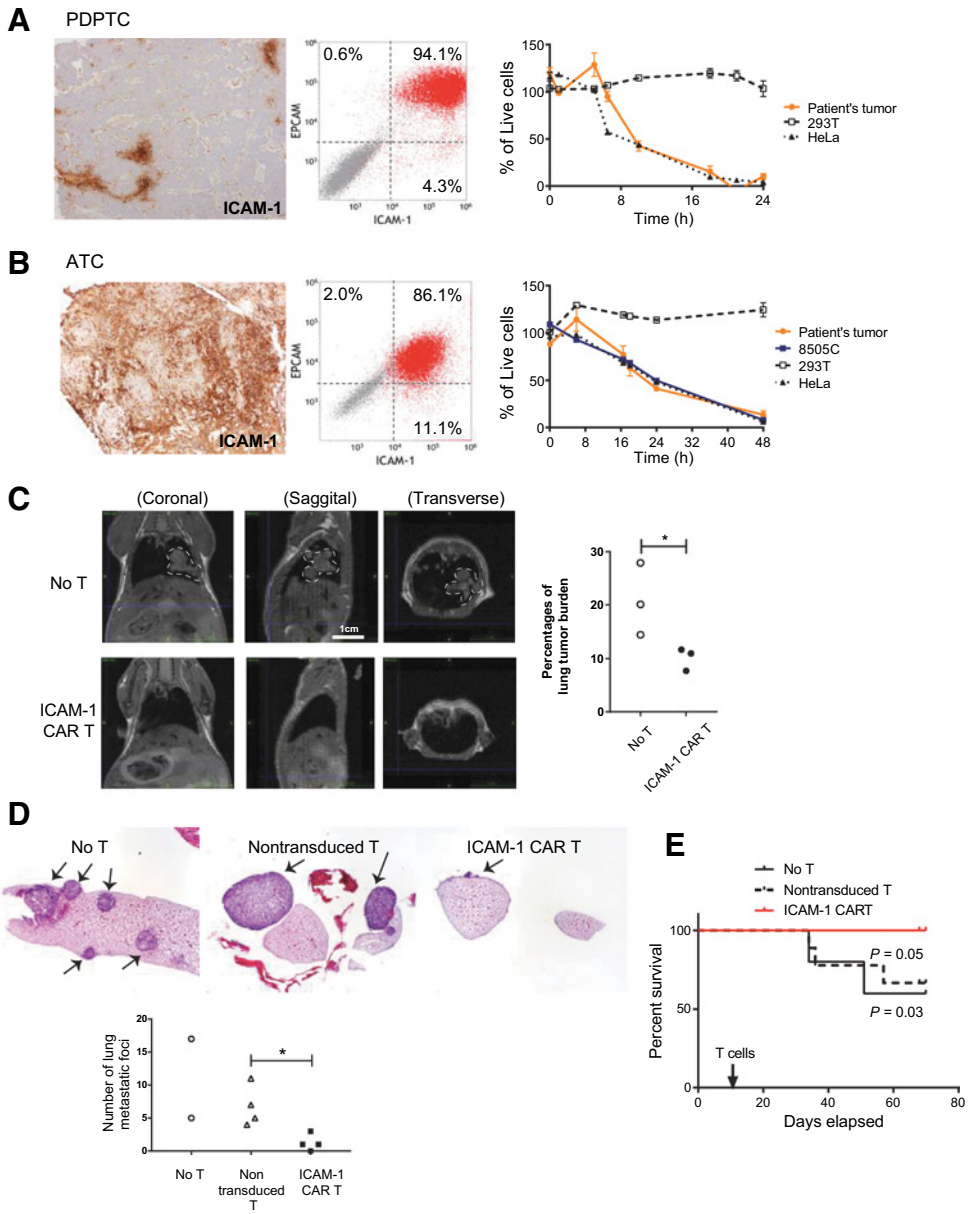

Figure 6.

Autologous ICAM-1 CAR T cells are effective in reducing tumor burden in thyroid cancer patient–derived tumor cells *in vitro* and *in vivo*. **A** and **B,** Tumors from PDPTC (**A**) and ATC (**B**) patients are analyzed by ICAM-1-specific IHC (10× magnification; left) and flow cytometry for EPCAM and ICAM-1 expression (middle). E: T assays using autologous ICAM-1 CAR T cells against primary tumors along with control 293T and HeLa cells are shown on the right. **C,** Single-cell resuspensions isolated from subcutaneous xenografts of ATC patient's primary cells (Supplementary Fig. S8) were intravenously injected into NSG mice for secondary transplantation. After 11 days, autologous ICAM-1 CAR T and nontransduced T cells were infused intravenously to assess therapeutic efficacy *in vivo*. T1 MRI analysis was carried out in no T cell and ICAM-1 CAR T groups at 67–72 days postxenograft to estimate tumor burden in the lung. Tumor outline is demarcated with white dotted lines. Quantification of the percentages of lung tumor burden was summarized and compared between no treatment and ICAM-1 CAR T treatment groups (*, $P < 0.05$; $n = 3$ per group). **D,** H&E staining of lung lobes in untreated, nontransduced T, and ICAM-1 CAR T administered animals. Numbers of lung tumor nodules were quantified and analyzed to assess significant differences between non-transduced T and ICAM-1 CAR T–treated animals (*, $P < 0.05$; $n = 3$ for no T and $n = 4$ for T-cell groups, one untreated mouse showed diffuse lung metastasis and therefore not quantified). **E,** Survival curves of ATC patient–derived tumor xenografted mice comparing no treatment, treatment with nontransduced T cells, and treatment with ICAM-1 CAR T cells up to 80 days postxenograft. Kaplan–Meier analysis was performed to assess statistical difference between different treatment groups ($n = 5$, 7, 10 for no T, nontransduced T, and ICAM-1 CAR T, respectively).

components of a third-generation CAR construct incorporating the CD28 and 4-1BB costimulatory domains (39). The R6.5 antibody (enlimomab) binds to the junction between the first and second domain of ICAM-1 and prevents interaction with LFA-1 (40). The R6.5 antibody has a proven safety and tolerability record with benefits for relieving inflammatory activity in patients

with rheumatoid arthritis, burn injuries, and transplant recipients (20–23). Its use for the treatment of stroke cases was associated with side effects due to a complement reaction attributable to the Fc portion of the mouse IgG2a (41). The F(ab) of R6.5 has an estimated affinity of 10 nmol/L (42), and the R6.5 scFv in the present ICAM-1 CAR T construct endowed T cells with ICAM-1 specific cytotoxicity that recognizes ICAM-1–overexpressing target tumor cells while sparing normal tissue with basal ICAM-1 expression.

In addition to its function as a tumor antigen, ICAM-1 possesses additional characteristics that can augment the antitumor activity of targeted CAR T cells. ICAM-1 is a well-documented inflammatory marker, and chronic inflammation has long been known to shape local and systemic immunity to promote an immunosuppressive tumor microenvironment and aid tumor development (43). Specifically, tumor-associated fibroblasts and tumor-associated macrophages are known to interact with tumor cells through ICAM-1 and promote cancer growth and metastasis (44, 45). Selective targeting of ICAM-1 expressing tumor and stroma by ICAM-1 CAR T may therefore yield synergistic antitumor activities when treating thyroid cancer, a strategy that has yielded positive results in a separate cancer model (46).

The marked enhancement of ICAM-1 expression in thyroid cancer cells upon addition of exogenous IFNγ suggests that its expression in advanced thyroid cancer cells *in vivo* is likely to increase upon antigen recognition and subsequent IFNγ release by infused ICAM-1 CAR T cells. In comparison, ICAM-1 expression is constitutively low in a variety of tissues, but its expression may be induced via proinflammatory cytokines such as IFNγ, TNFα, and IL1β in endothelial cells and other cell types (14, 33, 47, 48). Given that the IFNγ secretion by CAR T cells is a key indicator of their antitumor activity (49), concerns will arise over the possibility that paracrine IFNγ signaling may induce ICAM-1 expression in healthy neighboring cells, thus sensitizing them to CAR T-cell cytotoxicity. Activation of T cells via their native TCR requires a threshold density of peptide/MHC expression in order for sufficient signal propagation to occur (50). One strategy to further increase the therapeutic index of CAR T cells is lowering the CAR's antigen affinity to increase T-cell selectivity for targets with highly expressed antigens only while sparing normal cells with weaker expression. This hypothesis was tested and validated preclinically in prior studies using ERBB2 (HER2) and EGFR-directed CAR T cells (51, 52). Decreasing the R6.5 scFv affinity to that of typical TCR–pMHC interactions (1–100 μmol/L) may endow ICAM-1 CAR T cells with a similar ability to discriminate between ATC with high ICAM-1 overexpression and nonmalignant tissue cells with lower ICAM-1 expression. Dynamic ICAM-1 expression across various acute and chronic medical conditions including cytokine release syndrome (49, 53) warrant further investigation as certain comorbidities may amplify ICAM-1 expression resulting in an increased risk of on-target off-tumor toxicity. Optimizing strategies to increase the therapeutic index and to limit off-target toxicity will be crucial in bringing ICAM-1 CAR T into a clinical setting. Currently, we are in the process of developing affinity-tuned CAR T cells against ICAM-1–positive refractory thyroid cancers in preparation of a clinical trial to commence next year.

In conclusion, we report the first demonstration of robust and durable CAR T therapeutic effects in preclinical models of ATC using both cell lines and patient-derived tumors. The substantial surface and diffuse ICAM-1 expression patterns across almost all examined ATC samples demonstrate its potential as a target for CAR T therapies. ATC tumors are characterized by their heterogeneity, complex mutational landscape, and poor expression of molecules that have previously been exploited as molecular and cellular targets (1, 32, 54). The prolonged survival achieved upon treatment of ATC inoculated mice with ICAM-1 CAR T was particularly notable when compared with previous treatment strategies in preclinical metastatic models using the same ATC cell line (55–57). The preclinical xenograft model used here is limited by the inability to monitor potential toxicity mediated by ICAM-1 CAR against nontumor tissue. However, additional modifications with emerging technologies such as inducible CAR expression (58), CAR T-cell elimination via suicide gene activation (59), combinatorial antigen targeting (60), and affinity-tuned (51, 52) CAR T are likely to enhance safety while preserving on-target efficacy, thus providing a framework for adaptation of CAR T cells targeting ICAM-1 as a new treatment modality for advanced thyroid cancers and other solid tumors with ICAM-1 overexpression.

Disclosure of Potential Conflicts of Interest

No potential conflicts of interest were disclosed.

Authors' Contributions

Conception and design: I.M. Min, Y. Vedvyas, R. Zarnegar, T.J. Fahey, M.M. Jin
Development of methodology: I.M. Min, Y. Vedvyas, M. Zaman, M.M. Jin
Acquisition of data (provided animals, acquired and managed patients, provided facilities, etc.): I.M. Min, E. Shevlin, Y. Vedvyas, M. Zaman, B. Wyrwas, M.D. Moore, S. Park, S. Park, K.D. Gray, A.B. Tassler, T.J. Fahey, M.M. Jin
Analysis and interpretation of data (e.g., statistical analysis, biostatistics, computational analysis): I.M. Min, E. Shevlin, Y. Vedvyas, M. Zaman, T. Scognamiglio, M.D. Moore, S. Panjwani, T.J. Fahey, M.M. Jin
Writing, review, and/or revision of the manuscript: I.M. Min, E. Shevlin, Y. Vedvyas, M. Zaman, T. Scognamiglio, M.D. Moore, S. Park, S. Panjwani, K.D. Gray, A.B. Tassler, R. Zarnegar, T.J. Fahey, M.M. Jin
Administrative, technical, or material support (i.e., reporting or organizing data, constructing databases): I.M. Min, Y. Vedvyas, M. Zaman, W. Wang, M.M. Jin
Study supervision: I.M. Min, Y. Vedvyas, R. Zarnegar, T.J. Fahey, M.M. Jin

Acknowledgments

This work was supported by NIH grants P50 CA172012, R01CA178007, and Bite Me Cancer/American Thyroid Association award (ID-2016-052).

This work was supported by Weill Cornell Medicine's core facilities: the Translational Research Program, Flow cytometry, and the CITI Biomedical Imaging Center.

The costs of publication of this article were defrayed in part by the payment of page charges. This article must therefore be hereby marked *advertisement* in accordance with 18 U.S.C. Section 1734 solely to indicate this fact.

Received July 13, 2017; revised September 7, 2017; accepted September 28, 2017; published OnlineFirst October 12, 2017.

References

1. Xu B, Ghossein R. Genomic landscape of poorly differentiated and anaplastic thyroid carcinoma. Endocr Pathol 2016;27:205–12.
2. Siegel RL, Miller KD, Jemal A. Cancer Statistics, 2017. CA Cancer J Clin 2017;67:7–30.

3. Surveillance Epidemiology and End Results. SEER Cancer Stat Facts: Thyroid Cancer. Available from: https://seer.cancer.gov/statfacts/html/thyro.html.
4. Smallridge RC, Ain KB, Asa SL, Bible KC, Brierley JD, Burman KD, et al. American Thyroid Association guidelines for management of patients with anaplastic thyroid cancer. Thyroid 2012;22:1104–39.
5. Wagle N, Grabiner BC, Van Allen EM, Amin-Mansour A, Taylor-Weiner A, Rosenberg M, et al. Response and acquired resistance to everolimus in anaplastic thyroid cancer. N Engl J Med 2014;371:1426–33.
6. Rosove MH, Peddi PF, Glaspy JA. BRAF V600E inhibition in anaplastic thyroid cancer. N Engl J Med 2013;368:684–5.
7. Rosenberg SA, Restifo NP. Adoptive cell transfer as personalized immunotherapy for human cancer. Science 2015;348:62–8.
8. Haworth KB, Leddon JL, Chen CY, Horwitz EM, Mackall CL, Cripe TP. Going back to class I: MHC and immunotherapies for childhood cancer. Pediatr Blood Cancer 2015;62:571–6.
9. Gross G, Waks T, Eshhar Z. Expression of immunoglobulin-T-cell receptor chimeric molecules as functional receptors with antibody-type specificity. Proc Natl Acad Sci U S A 1989;86:10024–8.
10. Maher J, Brentjens RJ, Gunset G, Riviere I, Sadelain M. Human T-lymphocyte cytotoxicity and proliferation directed by a single chimeric TCRzeta /CD28 receptor. Nat Biotechnol 2002;20:70–5.
11. Milone MC, Fish JD, Carpenito C, Carroll RG, Binder GK, Teachey D, et al. Chimeric receptors containing CD137 signal transduction domains mediate enhanced survival of T cells and increased antileukemic efficacy in vivo. Mol Ther 2009;17:1453–64.
12. Maude SL, Frey N, Shaw PA, Aplenc R, Barrett DM, Bunin NJ, et al. Chimeric antigen receptor T cells for sustained remissions in leukemia. N Engl J Med 2014;371:1507–17.
13. Till BG, Jensen MC, Wang J, Qian X, Gopal AK, Maloney DG, et al. CD20-specific adoptive immunotherapy for lymphoma using a chimeric antigen receptor with both CD28 and 4-1BB domains: pilot clinical trial results. Blood 2012;119:3940–50.
14. Pober JS, Gimbrone MA Jr, Lapierre LA, Mendrick DL, Fiers W, Rothlein R, et al. Overlapping patterns of activation of human endothelial cells by interleukin 1, tumor necrosis factor, and immune interferon. J Immunol 1986;137:1893–6.
15. Schmidmaier R, Mrsdorf K, Baumann P, Emmerich B, Meinhardt G. Evidence for cell adhesion mediated drug resistance of multiple myeloma cells in vivo. Int J Biol Markers 2006;21:218–22.
16. Guo P, Huang J, Wang L, Jia D, Yang J, Dillon DA, et al. ICAM-1 as a molecular target for triple negative breast cancer. Proc Natl Acad Sci U S A 2014;111:14710–5.
17. Huang C, Li N, Li Z, Chang A, Chen Y, Zhao T, et al. Tumour-derived Interleukin 35 promotes pancreatic ductal adenocarcinoma cell extravasation and metastasis by inducing ICAM1 expression. Nat Commun 2017;8:14035.
18. Maruo Y, Gochi A, Kaihara A, Shimamura H, Yamada T, Tanaka N, et al. ICAM-1 expression and the soluble ICAM-1 level for evaluating the metastatic potential of gastric cancer. Int J Cancer 2002;100:486–90.
19. Kotteas EA, Boulas P, Gkiozos I, Tsagkouli S, Tsoukalas G, Syrigos KN. The intercellular cell adhesion molecule-1 (icam-1) in lung cancer: implications for disease progression and prognosis. Anticancer Res 2014;34:4665–72.
20. Kavanaugh AF, Davis LS, Jain RI, Nichols LA, Norris SH, Lipsky PE. A phase I/II open label study of the safety and efficacy of an anti-ICAM-1 (intercellular adhesion molecule-1; CD54) monoclonal antibody in early rheumatoid arthritis. J Rheumatol 1996;23:1338–44.
21. Cosimi AB, Conti D, Delmonico FL, Preffer FI, Wee SL, Rothlein R, et al. In vivo effects of monoclonal antibody to ICAM-1 (CD54) in nonhuman primates with renal allografts. J Immunol 1990;144:4604–12.
22. Mileski WJ, Burkhart D, Hunt JL, Kagan RJ, Saffle JR, Herndon DN, et al. Clinical effects of inhibiting leukocyte adhesion with monoclonal antibody to intercellular adhesion molecule-1 (enlimomab) in the treatment of partial-thickness burn injury. J Trauma 2003;54:950–8.
23. Enlimomab Acute Stroke Trial I. Use of anti-ICAM-1 therapy in ischemic stroke: results of the Enlimomab Acute Stroke Trial. Neurology 2001;57:1428–34.
24. Hansson M, Gimsing P, Badros A, Niskanen TM, Nahi H, Offner F, et al. A phase I dose-escalation study of antibody BI-505 in relapsed/refractory multiple myeloma. Clin Cancer Res 2015;21:2730–6.
25. Buitrago D, Keutgen XM, Crowley M, Filicori F, Aldailami H, Hoda R, et al. Intercellular adhesion molecule-1 (ICAM-1) is upregulated in aggressive papillary thyroid carcinoma. Ann Surg Oncol 2012;19:973–80.
26. Zhang KE, Ge SJ, Lin XY, Lv BB, Cao ZX, Li JM, et al. Intercellular adhesion molecule 1 is a sensitive and diagnostically useful immunohistochemical marker of papillary thyroid cancer (PTC) and of PTC-like nuclear alterations in Hashimoto's thyroiditis. Oncol Lett 2016;11:1722–30.
27. Vedvyas Y, Shevlin E, Zaman M, Min IM, Amor-Coarasa A, Park S, et al. Longitudinal PET imaging demonstrates biphasic CAR T cell responses in survivors. JCI Insight 2016;1:e90064.
28. Zhang L, Gaskins K, Yu Z, Xiong Y, Merino MJ, Kebebew E. An in vivo mouse model of metastatic human thyroid cancer. Thyroid 2014;24:695–704.
29. The Cancer Genome Atlas Research Network. Integrated genomic characterization of papillary thyroid carcinoma. Cell 2014;159:676–90.
30. Namba H, Nakashima M, Hayashi T, Hayashida N, Maeda S, Rogounovitch TI, et al. Clinical implication of hot spot BRAF mutation, V599E, in papillary thyroid cancers. J Clin Endocrinol Metab 2003;88:4393–7.
31. Pita JM, Figueiredo IF, Moura MM, Leite V, Cavaco BM. Cell cycle deregulation and TP53 and RAS mutations are major events in poorly differentiated and undifferentiated thyroid carcinomas. J Clin Endocrinol Metab 2014;99:E497–507.
32. Landa I, Ibrahimpasic T, Boucai L, Sinha R, Knauf JA, Shah RH, et al. Genomic and transcriptomic hallmarks of poorly differentiated and anaplastic thyroid cancers. J Clin Invest 2016;126:1052–66.
33. Smith CW, Rothlein R, Hughes BJ, Mariscalco MM, Rudloff HE, Schmalstieg FC, et al. Recognition of an endothelial determinant for CD 18-dependent human neutrophil adherence and transendothelial migration. J Clin Invest 1988;82:1746–56.
34. Uhlen M, Fagerberg L, Hallstrom BM, Lindskog C, Oksvold P, Mardinoglu A, et al. Proteomics. Tissue-based map of the human proteome. Science 2015;347:1260419.
35. Hayes SH, Seigel GM. Immunoreactivity of ICAM-1 in human tumors, metastases and normal tissues. Int J Clin Exp Pathol 2009;2:553–60.
36. Pilli T, Prasad KV, Jayarama S, Pacini F, Prabhakar BS. Potential utility and limitations of thyroid cancer cell lines as models for studying thyroid cancer. Thyroid 2009;19:1333–42.
37. Veitonmaki N, Hansson M, Zhan F, Sundberg A, Lofstedt T, Ljungars A, et al. A human ICAM-1 antibody isolated by a function-first approach has potent macrophage-dependent antimyeloma activity *in vivo*. Cancer Cell 2013;23:502–15.
38. Gao J, Aksoy BA, Dogrusoz U, Dresdner G, Gross B, Sumer SO, et al. Integrative analysis of complex cancer genomics and clinical profiles using the cBioPortal. Sci Signal 2013;6:pl1.
39. Carpenito C, Milone MC, Hassan R, Simonet JC, Lakhal M, Suhoski MM, et al. Control of large, established tumor xenografts with genetically retargeted human T cells containing CD28 and CD137 domains. Proc Natl Acad Sci U S A 2009;106:3360–5.
40. Staunton DE, Dustin ML, Erickson HP, Springer TA. The arrangement of the immunoglobulin-like domains of ICAM-1 and the binding sites for LFA-1 and rhinovirus. Cell 1990;61:243–54.
41. Vuorte J, Lindsberg PJ, Kaste M, Meri S, Jansson SE, Rothlein R, et al. Anti-ICAM-1 monoclonal antibody R6.5 (Enlimomab) promotes activation of neutrophils in whole blood. J Immunol 1999;162:2353–7.
42. Leelawattanachai J, Kwon KW, Michael P, Ting R, Kim JY, Jin MM. Side-by-side comparison of commonly used biomolecules that differ in size and affinity on tumor uptake and internalization. PLoS One 2015;10:e0124440.
43. Shalapour S, Karin M. Immunity, inflammation, and cancer: an eternal fight between good and evil. J Clin Invest 2015;125:3347–55.
44. Schellerer VS, Langheinrich M, Hohenberger W, Croner RS, Merkel S, Rau TT, et al. Tumor-associated fibroblasts isolated from colorectal cancer tissues exhibit increased ICAM-1 expression and affinity for monocytes. Oncol Rep 2014;31:255–61.
45. Yin M, Li X, Tan S, Zhou HJ, Ji W, Bellone S, et al. Tumor-associated macrophages drive spheroid formation during early transcoelomic metastasis of ovarian cancer. J Clin Invest 2016;126:4157–73.
46. Kakarla S, Chow KK, Mata M, Shaffer DR, Song XT, Wu MF, et al. Antitumor effects of chimeric receptor engineered human T cells directed to tumor stroma. Mol Ther 2013;21:1611–20.

Published OnlineFirst October 12, 2017; DOI: 10.1158/1078-0432.CCR-17-2008

47. Mickelson JK, Kukielka G, Bravenec JS, Mainolfi E, Rothlein R, Hawkins HK, et al. Differential expression and release of CD54 induced by cytokines. Hepatology 1995;22:866–75.
48. Lu Y, Yu T, Liang H, Wang J, Xie J, Shao J, et al. Nitric oxide inhibits heteroadhesion of cancer cells to endothelial cells: restraining circulating tumor cells from initiating metastatic cascade. Sci Rep 2014;4:4344.
49. Teachey DT, Lacey SF, Shaw PA, Melenhorst JJ, Maude SL, Frey N, et al. Identification of predictive biomarkers for cytokine release syndrome after chimeric antigen receptor T-cell therapy for acute lymphoblastic leukemia. Cancer Discov 2016;6:664–79.
50. Kalergis AM, Boucheron N, Doucey MA, Palmieri E, Goyarts EC, Vegh Z, et al. Efficient T cell activation requires an optimal dwell-time of interaction between the TCR and the pMHC complex. Nat Immunol 2001;2:229–34.
51. Liu X, Jiang S, Fang C, Yang S, Olalere D, Pequignot EC, et al. Affinity-tuned ErbB2 or EGFR chimeric antigen receptor T cells exhibit an increased therapeutic index against tumors in mice. Cancer Res 2015;75:3596–607.
52. Caruso HG, Hurton LV, Najjar A, Rushworth D, Ang S, Olivares S, et al. Tuning sensitivity of CAR to EGFR density limits recognition of normal tissue while maintaining potent antitumor activity. Cancer Res 2015; 75:3505–18.
53. Pinsky MR, Vincent JL, Deviere J, Alegre M, Kahn RJ, Dupont E. Serum cytokine levels in human septic shock. Relation to multiple-system organ failure and mortality. Chest 1993;103:565–75.
54. Ensinger C, Prommegger R, Kendler D, Gabriel M, Spizzo G, Mikuz G, et al. Her2/neu expression in poorly-differentiated and anaplastic thyroid carcinomas. Anticancer Res 2003;23:2349–53.
55. Sadowski SM, Boufraqech M, Zhang L, Mehta A, Kapur P, Zhang Y, et al. Torin2 targets dysregulated pathways in anaplastic thyroid cancer and inhibits tumor growth and metastasis. Oncotarget 2015;6:18038–49.
56. Mehta A, Zhang L, Boufraqech M, Liu-Chittenden Y, Zhang Y, Patel D, et al. Inhibition of survivin with YM155 induces durable tumor response in anaplastic thyroid cancer. Clin Cancer Res 2015;21:4123–32.
57. Bauerle KT, Schweppe RE, Lund G, Kotnis G, Deep G, Agarwal R, et al. Nuclear factor kappaB-dependent regulation of angiogenesis, and metastasis in an in vivo model of thyroid cancer is associated with secreted interleukin-8. J Clin Endocrinol Metab 2014;99:E1436–44.
58. Wu CY, Roybal KT, Puchner EM, Onuffer J, Lim WA. Remote control of therapeutic T cells through a small molecule-gated chimeric receptor. Science 2015;350:aab4077.
59. Di Stasi A, Tey SK, Dotti G, Fujita Y, Kennedy-Nasser A, Martinez C, et al. Inducible apoptosis as a safety switch for adoptive cell therapy. N Engl J Med 2011;365:1673–83.
60. Kloss CC, Condomines M, Cartellieri M, Bachmann M, Sadelain M. Combinatorial antigen recognition with balanced signaling promotes selective tumor eradication by engineered T cells. Nat Biotechnol 2013; 31:71–5.

Published OnlineFirst October 12, 2017; DOI: 10.1158/1078-0432.CCR-17-2008

Clinical Cancer Research

CAR T Therapy Targeting ICAM-1 Eliminates Advanced Human Thyroid Tumors

Irene M. Min, Enda Shevlin, Yogindra Vedvyas, et al.

Clin Cancer Res Published OnlineFirst October 12, 2017.